Physical characterization of amorphous In-Ga-Zn-O thin-film transistors with direct-contact asymmetric graphene electrode

Cite as: AIP Advances **4**, 097111 (2014); https://doi.org/10.1063/1.4895385
Submitted: 28 November 2013 • Accepted: 29 August 2014 • Published Online: 09 September 2014

Jaewook Jeong, Joonwoo Kim, Hee-Yeon Noh, et al.

Physical characterization of amorphous In-Ga-Zn-O thin-film transistors with direct-contact asymmetric graphene electrode

Jaewook Jeong,[1,a] Joonwoo Kim,[1] Hee-Yeon Noh,[1] Soon Moon Jeong,[1] Jung-Hye Kim,[1] and Sung Myung[2]
[1]*Division of Nano & Bio Technology, Daegu Gyeongbuk Institute of Science and Technology, Daegu, South Korea*
[2]*Thin Film Materials Research Group, Korea Research Institute of Chemical Technology, Daejeon 305-543, South Korea*

(Received 28 November 2013; accepted 29 August 2014; published online 9 September 2014)

High performance a-IGZO thin-film transistors (TFTs) are fabricated using an asymmetric graphene drain electrode structure. A-IGZO TFTs (channel length = 3 μm) were successfully demonstrated with a saturation field-effect mobility of 6.6 cm^2/Vs without additional processes between the graphene and a-IGZO layer. The graphene/a-IGZO junction exhibits Schottky characteristics and the contact property is affected not only by the Schottky barrier but also by the parasitic resistance from the depletion region under the graphene electrode. Therefore, to utilize the graphene layer as S/D electrodes for a-IGZO TFTs, an asymmetric electrode is essential, which can be easily applied to the conventional pixel electrode structure. [http://dx.doi.org/10.1063/1.4895385]

High-performance, stable amorphous InGaZnO (a-IGZO) thin-film transistors (TFTs) have been investigated widely for next-generation active-matrix devices.[1–3] The source/drain (S/D) electrodes for these TFTs should be determined carefully because the properties of the metal-semiconductor contact affect the device performance. Until now, Au/Ti,[3] Mo,[4] Al,[5] Cu,[6] MoW,[7] and Pt/Ti[8] have been used as S/D electrode materials, but these opaque electrodes are not appropriate for transparent pixel electrodes even though they exhibit good ohmic contact properties. For this reason, transparent S/D electrodes such as indium tin oxide (ITO)[9] and indium zinc oxide (IZO)[10,11] have been developed for a-IGZO TFTs. However, the production costs of these transparent electrodes are significant; indium is expensive material owing to its rareness. It is one of the important issues reducing the use of the rare-earth material for fabrication of displays and other related applications. In addition, the conventional transparent electrodes are brittle, which cannot be applied to flexible and stretchable electronic applications. Recently, a single-carbon graphene layer has been investigated as an alternative to the conventional transparent conducting materials for electrode applications,[12–16] because graphene exhibits semi-metal characteristics with a zero bandgap[15,17] and is expected to replace conventional indium-based transparent electrodes due to its high transparency and flexibility. In particular, there have been numerous efforts to use graphene as S/D electrodes in next-generation pixel electrodes in TFTs.[18–20] However, the underlying physics of the contact properties remain not well understood especially in oxide-based TFTs.

We fabricated a-IGZO TFTs using an asymmetric graphene electrode structure and analyzed the contact properties between the graphene and a-IGZO active layer (a-IGZO/graphene) through employing an additional probe electrode on the drain side. The asymmetric structure is essential to study the metal-semiconductor (M-S) junction characteristics of rectifying and blocking states

[a]E-mail : jjeong@dgist.ac.kr

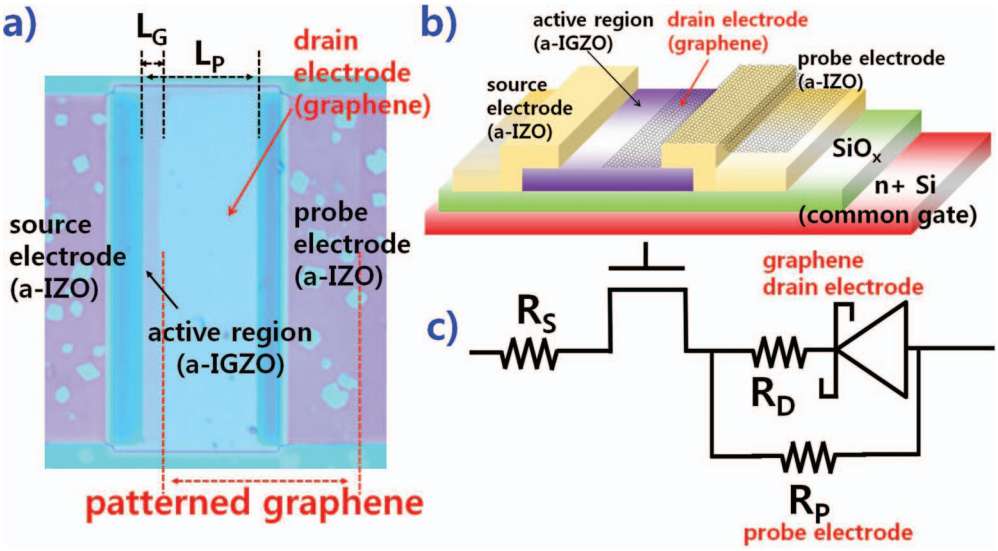

FIG. 1. (a) Top-side micrograph, (b) cross-sectional diagram, and (c) equivalent circuit model of the a-IGZO TFT with a graphene drain electrode.

depending on a polarity of applied drain voltage in TFTs. It also provides direct comparison of M-S junction characteristics between the conventional transparent electrode (a-IZO in this study) and the graphene using simple measurements. The probe electrode structure is useful for characterizing the contact properties between the a-IGZO/graphene layers and for confirming whether the graphene electrode functions as a real drain electrode. We found that the graphene/a-IGZO interface exhibits Schottky junction characteristics, and the contact properties can be significantly improved when the TFTs are operated under saturation conditions. Our results indicate that the a-IGZO/graphene combination can deliver high performance, low cost a-IGZO TFTs for various display applications without requiring additional fabrication processes.

A 30-nm-thick a-IGZO active layer (In:Ga:Zn = 1:1:1 by mol %) was deposited onto a 200-nm-thick silicon oxide layer (formed by wet annealing) by radio-frequency (RF) magnetron sputtering at room temperature. Active islands were patterned by photolithography and a buffered oxide etcher. The deposited layers were annealed in ambient oxygen for 2 h, followed by DC magnetron sputtering deposition of a 100-nm-thick source and probe a-IZO layer patterned by a lift-off process. The graphene layer was then transferred from the poly(methyl methacrylate) master which has a single graphene layer on it, and a graphene drain electrode was formed by reactive ion etching using oxygen plasma. To minimize the damage to the a-IGZO active region, low power, pressure, and gas flow process conditions (10W, 0.1 torr, and 10 sccm, respectively) were used. A Keithley 4200 semiconductor analyzer was used to measure the electrical characteristics.

Figures 1(a) and 1(b) shows the microscope image and schematic of the fabricated a-IGZO TFTs with asymmetric graphene electrodes, respectively. The channel length and probe length from the source to the patterned graphene drain (L_G) and from the source to the probe (L_P) are defined as shown in Fig. 1(a), respectively: L_G was fixed at 3 μm, while L_P was varied from 8 to 100 μm. The equivalent circuit model, shown in Fig. 1(c), includes the parallel connection of the Schottky diode and resistance components that represent the graphene drain and probe electrodes, respectively.

Firstly, we measured the transfer characteristics of the a-IGZO TFTs without the graphene as shown in Fig. 2(a). Conventional transfer curves were obtained with a large on/off current ratio, small subthreshold, and linear and saturation field-effect mobility values of 10.6 and 8.9 $cm^2 \cdot V^{-1} \cdot s^{-1}$, respectively. The electrical characteristics of the graphene transferred to the a-IGZO TFT prior to S/D electrodes patterning are shown in Fig. 2(b). The measurement was performed through the a-IZO source and probe electrodes (probe width-to-length ratio $W/L_P = 60/100$) through the application of different gate–source voltages (V_{GS}). It was shown that most of the probe current originated from the

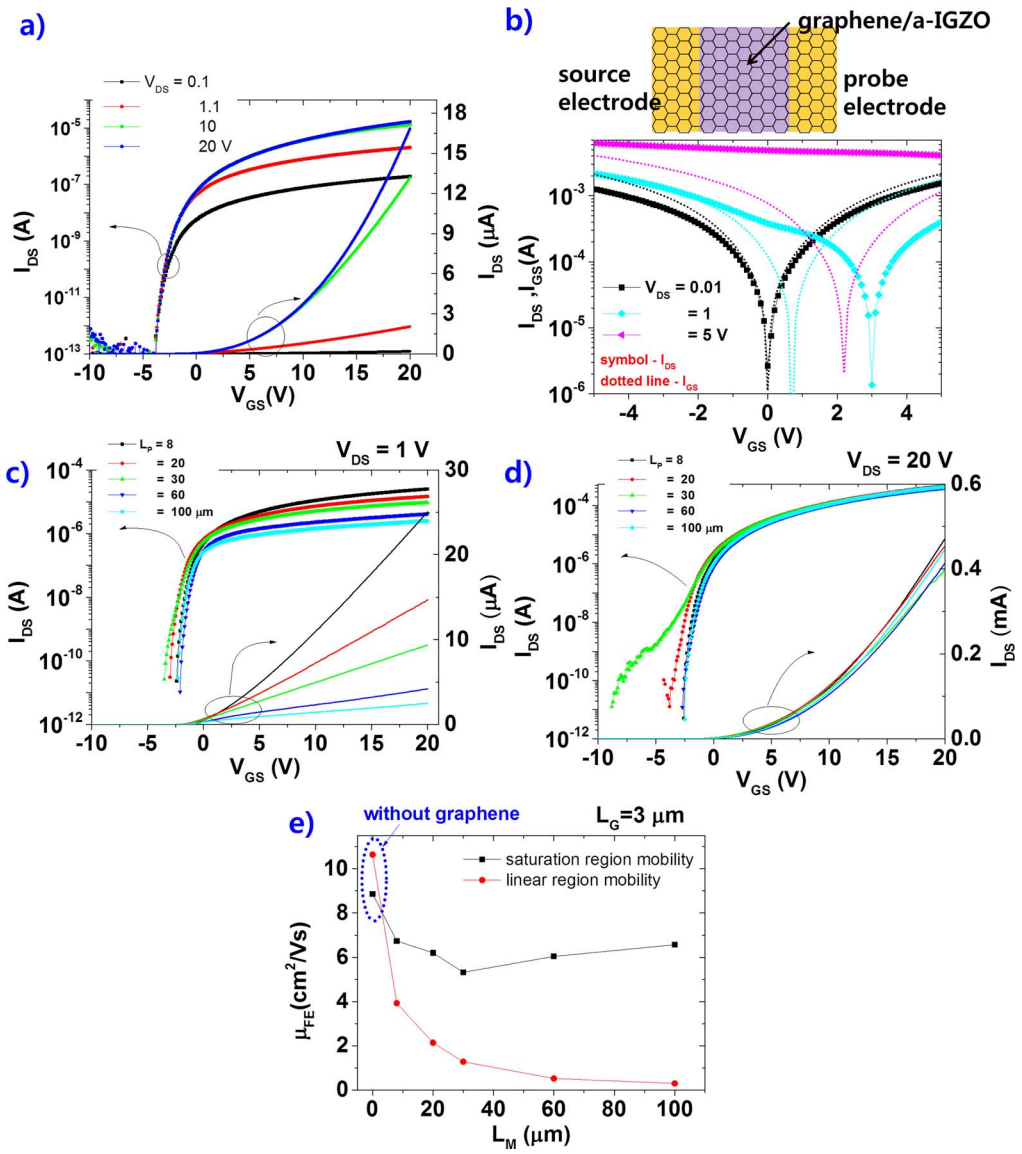

FIG. 2. (a) Transfer characteristics of the a-IGZO TFT without graphene (W/L = 60/100). In this case, the probe electrode functions as a drain electrode. (b) Transfer characteristics of the graphene on the a-IGZO TFT before patterning (top drawing is a structure for measurements). Transfer characteristics of the a-IGZO TFTs after patterning of the graphene sheet in the (c) linear region (V_{DS} = 1 V) and (d) saturation region (V_{DS} = 20 V). (e) Field-effect mobility of the a-IGZO TFTs as a function of L_P in the linear and saturation regions.

gate leakage current (dotted line), particularly when the probe-source voltage (V_{PS}) was low, which indicates that the adhesion of the graphene and a-IGZO was sufficient even though it originated from weak van der Waals forces. For a large V_{PS}, the current level increased significantly because the source-to-probe current became dominant and the current level represented the conductivity of the graphene. After patterning of the graphene, the TFTs exhibited clear transfer characteristics at a drain-source voltage (V_{DS}) = 1 V with a high on/off current ratio, as shown in Fig. 2(c). It should be noted that if graphene is a good conductor and forms good ohmic contact, then the transfer curve will exhibit the same characteristics for different L_P values because L_P is always larger than L_G in the proposed structure. However, the dependence on L_P seen in Fig. 2(c) revealed that the graphene electrode did not behave perfectly as a drain electrode. The current partially flowed to the probe electrode even when L_P was much larger than L_G. This situation changed when V_{DS} increased to

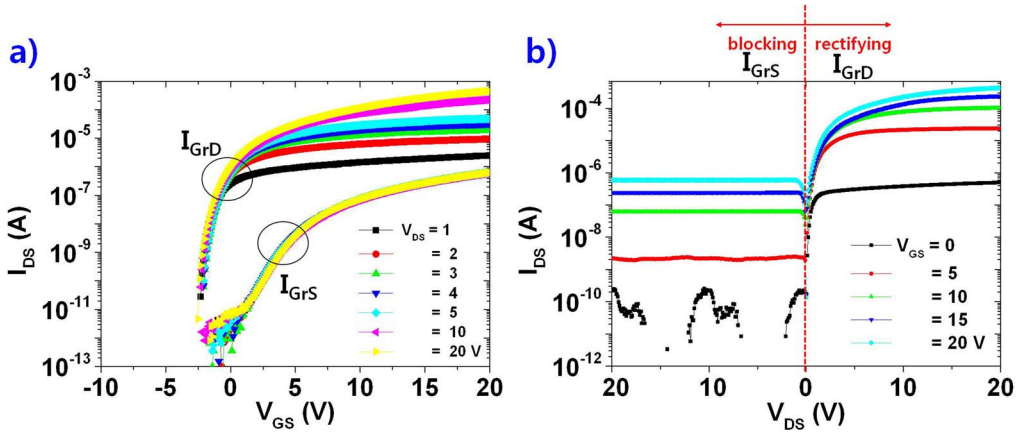

FIG. 3. (a) Transfer and (b) output characteristics of the a-IGZO TFTs for different S/D connections (GrD and GrS).

20 V (Figure 2(d)), where it can be seen that the drain currents are the same for different values of L_P. These characteristics are summarized by extracting the field-effect mobilities in the linear and saturation regions (μ_{FE_lin} and μ_{FE_sat}, respectively):

$$\mu_{FE\_lin}(V_{GS}) = \frac{L_G}{C_{ins} W V_{DS}} \frac{\Delta I_{DS}}{\Delta V_{GS}} \tag{1}$$

$$\mu_{FE\_sat}(V_{GS}) = \frac{2L_G}{C_{ins} W} \left(\frac{\Delta \sqrt{I_{DS}}}{\Delta V_{GS}} \right)^2 \tag{2}$$

Here, C_{ins} is the capacitance of the gate insulator per unit area, and the Δ/Δ operator denotes a least-squares fitting with a V_{GS} value ranging from 5 to 20 V. Figure 2(e) shows the field-effect mobilities in the linear ($V_{DS} = 1$ V) and saturation ($V_{DS} = 20$ V) regions. The field-effect mobilities in the linear region decrease as L_P increases, whereas they remain relatively constant near 6.6 $cm^2 \cdot V^{-1} \cdot s^{-1}$ in the saturation region. It should be noted that even though the field-effect mobility value decreased after forming the graphene drain electrode in the linear region, the saturation field-effect mobility value of a-IGZO TFT with the graphene remained high considering that the channel length was significantly shorter than the that of a-IGZO TFT without graphene (100 *vs.* 3 μm). Based on the L_P dependency, the graphene electrode only functioned as a perfect drain electrode when V_{DS} was large.

Further analyses were performed by switching the connections of the S/D electrodes. Figures 3(a) and 3(b) shows the transfer and output characteristics of the a-IGZO TFTs for the drain and source side connections of the graphene electrode, denoted as GrD and GrS, respectively. The drain current of the GrS connection (I_{GrS}) decreased significantly in comparison with that of the GrD connection (I_{GrD}), and for the GrS connection, the current level was nearly invariant with respect to V_{DS}. In this case, we expect transfer curves with conventional long-channel TFT characteristics due to the probe electrode. However, a severe decrease in the drain current and a lack of dependence on V_{DS} was observed, which is frequently observed when the parasitic resistance is extremely large. The output characteristics showed conventional diode-like characteristics, with the GrD connection exhibited rectifying characteristics and the GrS connection exhibited blocking characteristics similar to those of the Schottky diode. This indicated clearly that the Schottky diode of the equivalent circuit model shown in Fig. 1(c) was dominant due to the large Schottky barrier height between the graphene and a-IGZO. Thus, if graphene is used on both sides of the S/D electrodes, then the a-IGZO TFT performance will be severely decreased because there will always be a blocking state on one side. Accordingly, these observations explain the low field-effect mobilities of a-IGZO TFTs with S/D graphene electrodes if there are no additional processes.[20]

Figure 4(a) shows the temperature-dependent transfer characteristics of the a-IGZO TFTs with a GrD connection ($W/L_P = 60/30$) for $V_{DS} = 1$ V; only slightly thermally activated behavior was

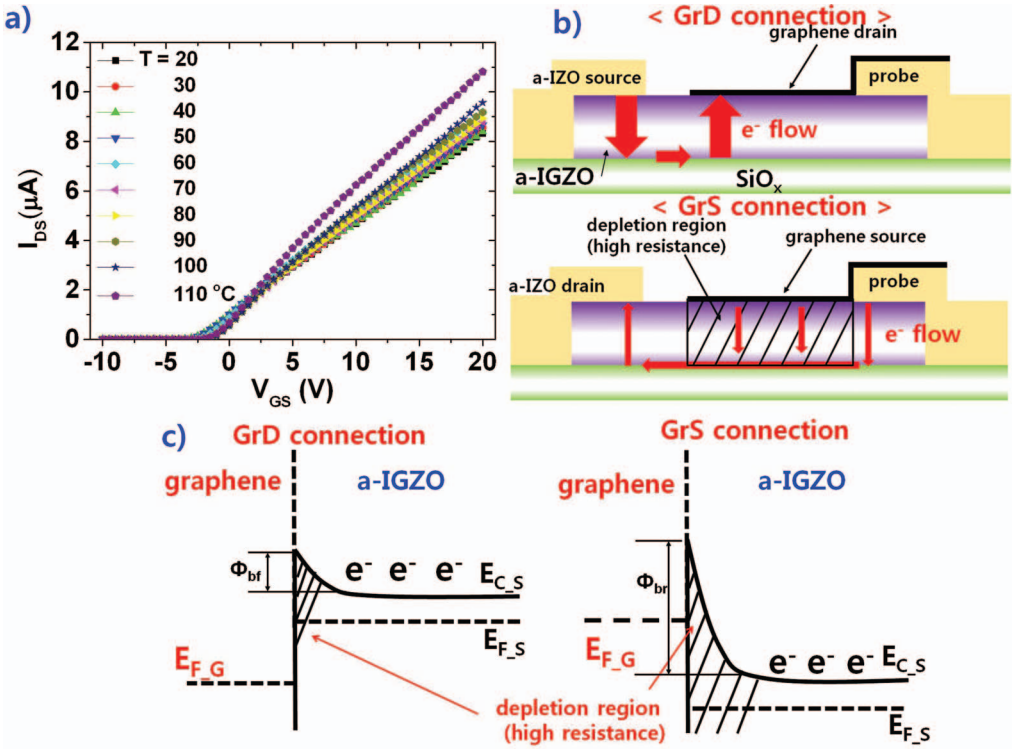

FIG. 4. (a) Transfer characteristics of the a-IGZO TFTs with a graphene drain electrode for temperatures ranging from 20 to 110 °C. (b) Cross-sectional diagram of the current flow and (c) band alignment of the a-IGZO TFT structure near the S/D electrodes for the GrD and GrS connections. (E_{F_G} is the Fermi level of the graphene, and E_{C_S} and E_{F_S} are the conduction band edge and Fermi level of the a-IGZO active layer, respectively.)

observed. For the low V_{DS} condition, because the Schottky barrier is a bottleneck in the current flow, the Schottky barrier height (Φ_b) can be estimated from the data using the thermionic current equation, as follows:

$$\frac{J}{T^2} = A \exp\left(-\frac{q\Phi_b}{kT}\right) \tag{3}$$

where J is the current density, T is the temperature, and A is a proportionality constant including the Richardson constant. However, negative height values were obtained when it was assumed that the Schottky diode in Fig. 1(c) was the dominant influence on the drain current (data not shown here), i.e., the Schottky barrier effect was overestimated. The Schottky barrier is not the only origin of low drain currents at low V_{DS}, and it is speculated that the formation of a high-resistance depletion bulk region under the graphene electrode may also be responsible, which would explain the transfer curves being relatively independent of the temperature. Although the barrier height decreased as the temperature increased, the resistance of the depletion region remained quite high and induced a high parasitic resistance in the bulk region. In the saturation region with the GrD connection, the barrier height was low and the corresponding carrier density in the bulk region was high; thus the graphene functioned as a real electrode, as shown in Fig. 4(b). In this case, high field-effect mobilities were obtained due to the low Schottky barrier height and low resistance in the bulk region. However, for the GrS connection, the carrier density in the bulk region was low resulting in the formation of a high-resistance region blocked the flow of the drain current, as shown in Figs. 4(b). Figure 4(c) shows a band alignment between the graphene and a-IGZO active layer. For the GrD connection, there is a small Schottky barrier (Φ_{bf}) which allows electron flows from the a-IGZO active layer to the graphene electrode. On the contrary, for the GrS connection, the increase in the Schottky barrier (Φ_{br}) blocks the electron flows from the graphene electrode to the a-IGZO active layer. In this

case, the active region is fully depleted by reverse voltage of M-S junction resulting in a significant increase of resistance of the active region. The depletion region as well as the Schottky barrier blocks the electron flows inducing a significant decrease of the drain current for the GrS connection. Based on this analysis, the low performance of the a-IGZO TFTs with the GrS connection resulted from the formation of a high-resistance bulk region under the graphene electrode, even though there was an additional probe electrode.

In conclusion, high-performance a-IGZO TFTs using graphene electrodes can be achieved with an asymmetric S/D electrode structure. The maximum field-effect mobility in the saturation operation region was approximately 6.6 $cm^2 \cdot V^{-1} \cdot s^{-1}$. Because a-IGZO TFTs are affected by the Schottky barrier and the formation of a depletion region under the graphene electrode, high field-effect mobility can only be obtained when the TFTs are operated in the saturation region. We believe that our results provide a physical understanding of fabricating high-performance oxide-based devices for graphene pixel electrodes in various display applications.

This work was supported by the National Research Foundation of Korea (NRF) grant funded by the Korea government (MSIP) (No. 2014R1A2A2A01006588). It was also supported by the DGIST R&D Program of the Ministry of Science, ICT and Technology of Korea (14-NB-04).

[1] K. Nomura, H. Ohta, A. Takagi, T. Kamiya, M. Hirano, and H. Hosono, Nature(London) **432**, 488 (2004).
[2] A. Suresh, P. Wellenius, A. Dhawan, and J. Mutha, Appl. Phys. Lett. **90**, 123512 (2007).
[3] H. Yabuta, M. Sano, K. Abe, T. Aiba, T. Den, H. Kumomi, K. Nomura, T. Kamiya, and H. Hosono, Appl. Phys. Lett. **89**, 112123 (2006).
[4] J. Park, C. Kim, S. Kim, I. Song, S. Kim, D. Kang, H. Lim, H. Yin, R. Jung, E. Lee, J. Lee, K.-W. Kwon, and Y. Park, IEEE Electron Device Lett. **29**, 879 (2008).
[5] J. H. Na, M. Kitamura, and Y. Arakawa, Appl. Phys. Lett. **93**, 063501 (2006).
[6] J. Jeong, G. J. Lee, J. Kim, and B. Choi, Appl. Phys. Lett. **100**, 112109 (2012).
[7] M. Kim, J. H. Jeong, H. J. Lee, T. K. Ahn, H. S. Shin, J. S. Park, J. K. Jeong, Y. G. Mo, and H. D. Kim, Appl. Phys. Lett. **90**, 212114 (2007).
[8] J. S. Park, J. K. Jeong, Y. G. Mo, H. D. Kim, and S. I. Kim, Appl. Phys. Lett. **90**, 262106 (2007).
[9] A. Suresh and J. F. Muth, Appl. Phys. Lett. **92**,033502 (2008).
[10] J. K. Jeong, J. H. Jeong, H. W. Yang, J.-S. Park, Y.-G. Mob, and H. D. Kim, Appl. Phys. Lett. **91**, 113505 (2007).
[11] J. Jeong, G. J. Lee, J. Kim, S. M. Jeong, and J.-H. Kim , J. Appl. Phys. **114**, 094502 (2013).
[12] K. S. Novoselov, A. K. Geim, S. V. Morozov, D. Jiang, M. I. Katsnelson, I. V. Grigorieva, S. V. Dubonos and A. A. Firsov, Nature **438**, 197 (2005).
[13] A. K. Geim, K. S. Novoselov, Nat. Mater. **6**, 183 (2007).
[14] X. Li, W. Cai, J. An, S. Kim, J. Nah, D. Yang, R. Piner, A. Velamakanni, I. Jung, E. Tutuc, S. K. Banerjee, L. Colombo, R. S. Ruoff, Science **324**, 1312 (2009).
[15] A. C. Ferrari, J. C. Meyer, V. Scardaci, C. Casiraghi, M. Lazzeri, F. Mauri, S. Piscanec, D. Jiang, K. S. Novoselov, S. Roth, and A. K. Geim, Phys. Rev. Lett. **97**, 187401 (2006).
[16] X. Li, H. Zhu, K. Wang, A. Cao, J. Wei, C. Li, Y. Jia, Z. Li, X. Li, and D. Wu, Adv. Mater. **22**, 2743 (2010).
[17] G. Giovannetti, P. A. Khomyakov, G. Brocks, P. J. Kelly, and J. Brink, Phys. Rev. B: Condens. Matter **76**, 073103 (2007).
[18] C. Di, D. Wei, G. Yu, Y. Liu, Y. Guo, and D. Zhu, Adv. Mater. **20**, 3289 (2008).
[19] D. Seo, S. Jeon, S. Seo, I. Song, C. Kim, S. Park, J. S. Harris, and U.-I. Chung, Appl. Phys. Lett. **97**, 172106 (2010).
[20] J. E. Lee, B. K. Sharma, S.-K. Lee, H. Jeon, B. H. Hong, H.-J. Lee, and J.-H. Ahn, Appl. Phys. Lett. **102**, 113112 (2013).